scientific reports

Check for updates

OPEN

Flue gas desulfurization gypsum mineralization in waste Lye medium at pilot scale

Yuliang Cao[1,3], Tingfeng Liu[1,3], Guodong Chen[1,3] & Wenyi Tan[1,2,3]✉

CO_2 capture, utilization and sequestration technology is currently a global research hotspot with increasing CO_2 emission and rising atmospheric temperatures. Flue gas desulfurization gypsum (FGDG) was used to realize CO_2 mineralization in waste NaOH lye in a pilot scale bubble tower. The effects of the ionic strength, CO_2 flow rate, reaction temperature, and liquid level in the reactor on the properties of the mineralization products and the CO_2 mineralization efficiency were investigated using thermogravimetric analysis, X-ray diffraction (XRD), scanning electron microscopy (SEM), and particle size analysis. The experimental results indicated that ionic strength, reaction temperature and CO_2 flow rate significantly influenced the CO_2 mineralization efficiency of FGDG. The CO_2 mineralization efficiency reached 92.15% under the optimized conditions (the ionic strength: 10^{-2} mol·L^{-1}, CO_2 flow rate: 20 L·h^{-1}, reaction temperature: 60 °C, liquid level: 50 cm). The liquid level has a strong effect on the particle size distribution of mineralized products. A higher liquid level promotes the formation of mineralized products with smaller particle sizes. These products consist of a single cluster of crystals and the main component is calcium carbonate. The pilot scale results demonstrate optimized evidence for CO_2 mineralization using FGDG in waste lye. Therefore, this approach enables the comprehensive utilization of three types of waste-gas, liquid, solid- generated produced in coal-fired power plants.

Keywords Flue gas desulfurization gypsum (FGDG), Waste Lye, Pilot scale reactor, CO_2 mineralization

The use of fossil energy emits large amounts of greenhouse gases (e.g., CO_2, CH_4, N_2O and O_3) due to the continuous development of global industrialization. These emissions have contributed significantly to global warming, posing a severe threat to the ecological environment as well as the human survival[1,2]. Consequently, reducing CO_2 emissions has garnered increasing attention[3,4]. CO_2 capture, utilization and sequestration (CCUS) is currently a necessary approach to achieve CO_2 emission reduction[5]. Among CCUS technologies, mineral sequestration (mineralization) is particularly promising, as it generates stable carbonate products that ensure permanent, safe and efficient CO_2 storage with minimal leakage risk[6]. This technology achieves CO_2 mineralization by precipitating stable carbonate compounds, such as calcium carbonate and magnesium carbonate[7,8].

Certain natural minerals and industrial solid wastes containing abundant of Ca^{2+} have been explored as feedstocks for mineralization. However, CO_2 mineralization using natural minerals requires harsh conditions, and the associated mining, milling, and separation processes make it costly[9]. In contrast, industrial solid wastes such as fly ash[10,11], waste gypsum[12–14], steel slag[15], and calcium carbide slag[16] are considered highly promising due to their high reactivity, widespread availability, and lower costs.

Flue gas desulfurization gypsum (FGDG), a byproduct of the wet flue gas desulfurization process in coal-fired power plants, is primarily composed of $CaSO_4{\cdot}2H_2O$, with a content up to 93%. Currently, China's annual FGDG emissions are approximately 80 million tons, with a utilization rate of 78%, and an annual stockpile of around 100 million tons[17]. CO_2 mineralization using FGDG has been extensively studied at the laboratory scale. For instance, Lee used direct wet mineralization of FGDG to investigate the effects of process parameters, such as ammonia concentration, CO_2 flow rate, and solid-liquid ratio, on the conversion rate and CO_2 mineralization efficiency[18]. Wing et al. proposed an ultrasonic technique to study the effects of different liquid media on the mineralization process and the crystalline morphology of the products[12,19]. Ding explored the mineralization of CO_2 by FGDG mineralization in an NH_4Cl-H_2O system based on the solubility equilibrium theory between a salt solution and an insoluble electrolyte, achieving a 98% carbonation rate and demonstrating the recyclability of the carbonation reaction filtrate[20]. Wang proposed an amine-promoted carbonation process for waste gypsum,

[1]School of Mechanical Engineering, Nanjing Institute of Technology, Nanjing 211167, Jiangsu, China. [2]Xuzhou University of Technology, Xuzhou 221018, Jiangsu, China. [3]International Joint Laboratory of Green and Low Carbon Development, Jiangsu Province, China. ✉email: twy1102@gmail.com

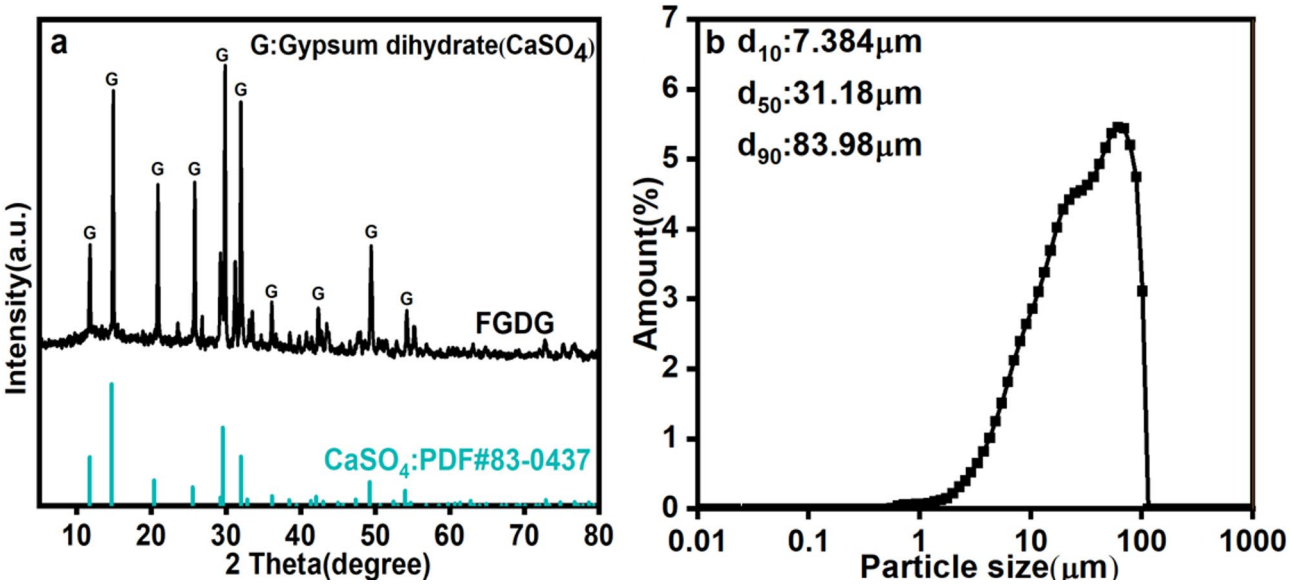

Fig. 1. (**a**) XRD pattern of FGDG and (**b**) the particle size distribution of FGDG.

Material	CaO	SO_3	SiO_2	Al_2O_3	MgO	Na_2O	K_2O	LOI*
wt%	46.02	46.15	3.6	1.56	0.55	0.17	0.26	1.69

Table 1. Chemical composition of FGDG.

coupled with amine regeneration using bipolar membrane electrodialysis (BMED), and evaluated seven types of amines as reaction media for CO_2 mineralization[21]. Chang et al. proposed using waste lye from steel smelting and steel slag as raw materials for mineralization to absorb CO_2, which not only reduces water consumption but also lowers the total cost[22]. However, the waste lye utilized contains a lot of impurities, resulting in a complex composition of the product. Kumar et al. investigated carbonation of the waste lye produced by the paper industry to, achieving simultaneous CO_2 absorption and recovery of carboxylic acids and lignin, though the CO_2 capture performance remained unevaluated in this process[23].

Many studies have focused on liquid alkaline media, including ammonia or organic amines, for CO_2 mineralization, which is severely limited by the cost of liquid media. Few studies have explored the application of waste lye so far, despite its availability and cost advantages. It is well known that ionic strength positively influences reaction rates in reactors[24,25]. Altiner et al. adopted NaOH and $Ca(OH)_2$ in a "two-step" carbon sequestration method, but focused primarily on performance outcomes rather than the effects of ionic strength[14].

The study demonstrates a pilot scale system to achieve CO_2 mineralization and to recycle product. The effects of key parameters such as ionic strength in solution, CO_2 flow rate, reaction temperature and liquid level on the CO_2 mineralization efficiency of FGDG were systematically investigated. And the particle size and morphology of the products was characterized by means of XRD, TG, SEM, and particle size analysis. A comprehensive utilization of three kinds of wastes (gas CO_2, solid FGDG and liquid waste lye) emitted from the coal-fired power plants was explored Furthermore, both inherent factors (e.g., ionic strength) and external factors (e.g., reactor structure) of CO_2 mineralization at the pilot scale are discussed in detail.

Materials and methodology

Materials

The FGDG used in this study was produced from a coal-fired power plant. The FGDG sample was first dried at 105 °C for 8 h to remove surface moisture and then sieved to 60 mesh[26]. The purity of the $CaSO_4$ in the FGDG used was 97%, as determined by wet analysis. The phase composition of the samples was analyzed by X-ray diffraction (XRD, Bruker D2 Advance with a Cu Kα source at 30 kV and 10 mA) with the scanning scope (2θ) from 5° to 80° under the speed of 10° min^{-1} and the obtained patterns were examined using jade6.5 (PDF#83-0437) software for mineral identification. The XRD confirmed that the main component of the FGDG samples was calcium sulfate dihydrate, as shown in Fig. 1a. The particle size was measured with a particle size analyzer (Bettersize 3000 Plus), and the average size of the FGDG samples (d_{50}) was 31.18 μm, with 90% of the particles smaller than 83.98 μm, as shown in Fig. 1b. The composition of the sample was analyzed via X-ray fluorescence (XRF, ZSX Primuss II, Rigaku), and the FGDG impurities were mainly SiO_2 and Al_2O_3, as shown in Table 1. The theoretical CaO content in pure $CaSO_4{\cdot}2H_2O$ is ~ 32.5% (based on molar mass ratios), but the higher CaO content (46.02%) reflects the dehydration of gypsum (loss of crystalline water) during sample preparation (dried

at 105 °C for 8 h) and potential partial decomposition of $CaSO_4{\cdot}2H_2O$ into CaO and SO_3. This aligned with the XRD results as Fig. 1a, confirming $CaSO_4{\cdot}2H_2O$ as the dominant phase.

CO_2 mineralization experiment

NaOH solutions with different ionic strengths were prepared to simulate the waste lye, and the ionic strength of the waste lye was calculated according to the Eq. (1):

$$I = \frac{1}{2}\sum_{i=1}^{n} C_i Z_i{}^2 \tag{1}$$

Here, I is the ionic strength of the waste lye, C_i is the ion concentration, and Z_i is the charge number of ions.

The waste lye was pumped into the pilot scale reactor with a height of 120 cm, an inner diameter of 15 cm and a length of the sampling tube 50 cm, as shown in Fig. 2a. The physical diagram of the reactor is shown in Fig. 2b. After the waste lye was heated to the desired temperature, a weighed FGDG sample was added to the waste lye through the auger to prepare slurry, and then 99% CO_2 gas was bubbled into the slurry with vigorous stirring. The mineralization reaction process is shown in Fig. 3. According to the standards for industrial production waste lye, equipment limitations and energy-saving requirements, the effects of reaction temperature (40 °C, 60 °C, 80 °C), ionic strength (10^{-12} mol·L^{-1}, 5×10^{-9} mol·L^{-1}, 10^{-2} mol·L^{-1}), CO_2 flow rate (20 L·h^{-1}, 40 L·h^{-1}, 60 L·h^{-1}) and liquid level (30 cm, 40 cm, 50 cm) on FGDG mineralization were investigated[34]. The detailed experimental conditions are shown in Table 2. For example, for $I_{10}{}^{-12}$-T40-r20-h30, the experiment was carried out at I = 10^{-12} mol·L^{-1}, a reaction temperature of 40 °C, a CO_2 flow rate of 20 L·h^{-1} and a liquid level of 30 cm. Samples were taken from the exit at a given reaction time for determination (2, 4, 6, 15, 30, and 60 min), and the pH was measured at various reaction time points (2, 4, 6, 8, 10, 15, 20, 25, 30, 40, 50, and 60 min).

Characterization of the product and calculation of the storage capacity

All the samples were separated from the liquid by a high-speed centrifuge, and the obtained solid samples were dried at 180 °C for 8 h. The purity of the $CaCO_3$ in the product was calculated from the weight loss of the solid samples during the thermogravimetric process which was increased from 600 °C to 780 °C under N_2 atmosphere conditions. Pane and Lin concluded that the decomposition of $CaCO_3$ occurred at 600 °C to 780°C[27,28]. A particle size analyzer (Bettersize 3000 Plus) was used to determine the particle size distribution of the mineralization products.

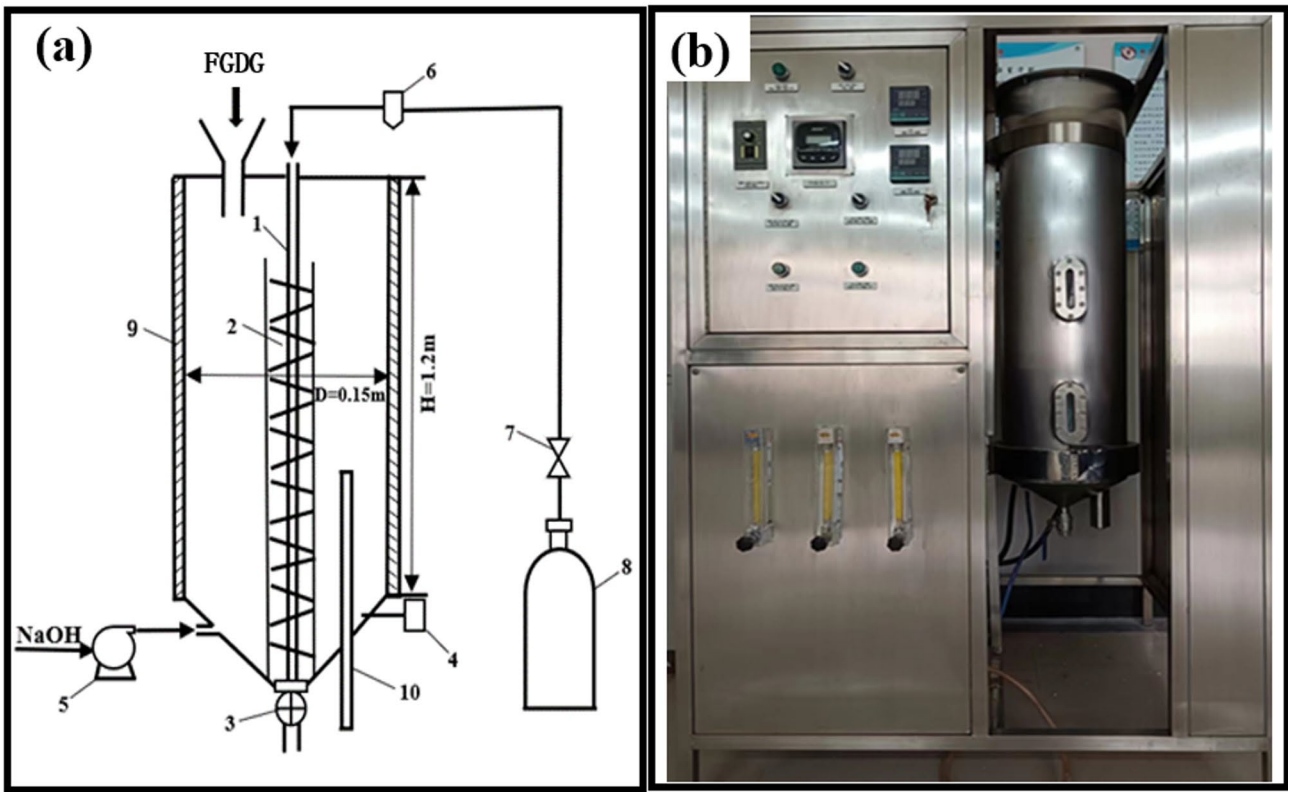

Fig. 2. (**a**) Structure of a pilot scale mineralization reactor: 1—gas tubes, 2—heating coils, 3—valve, 4—pH meter, 5—liquid pump, 6—gas flow meter, 7—gas pressure reducing valves, 8—CO_2 cylinders, 9—insulation, 10—sampling tube. (**b**) Physical drawings of a pilot scale mineralization reactor.

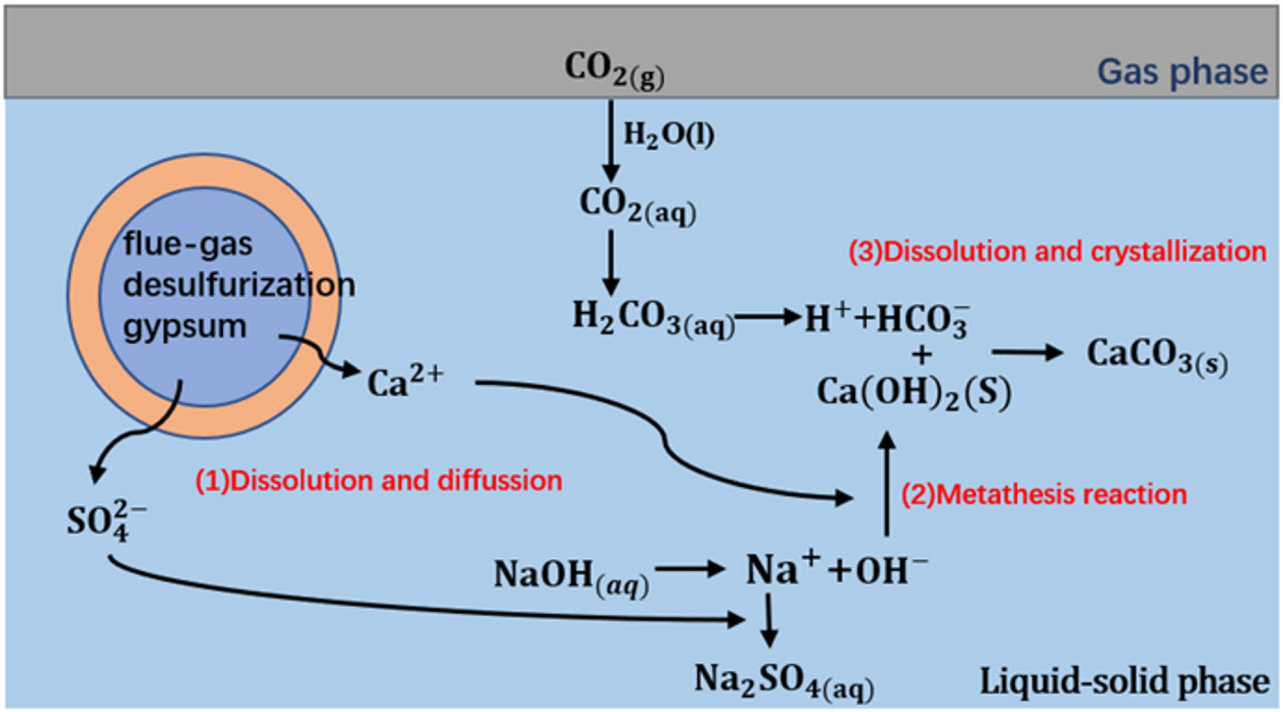

Fig. 3. Schematic diagram of carbonization and carbon sequestration of FGDG.

Reaction condition	1	2	3
Temperature, T/°C	40	60	80
Ionic strengths, I/mol·L^{-1}	10^{-12}	5×10^{-9}	10^{-2}
CO_2 flow rate, r/L·h^{-1}	20	40	60
liquid level, h/cm	30	40	50

Table 2. Reaction conditions in the pilot scale experiments.

The morphology of the products was observed by scanning electron microscopy (National Ceremony SEM 4000). The mass of $CaCO_3$ in the sample at time t is calculated via the following Eq. (2):

$$m_{t-CaCO_3} = \frac{\Delta m_{co_2}}{M_{co_2}} \times M_{CaCO_3} \tag{2}$$

Where Δm_{co_2} is the weight of CO_2 that escapes when $CaCO_3$ decomposes during thermogravimetry and where m_{t-CaCO_3} is the mass of $CaCO_3$ in the sample of products. M_{caco3} is the relative molecular weight of $CaCO_3$ and M_{CO_2} is the relative molecular weight of CO_2. The purity of the $CaCO_3$ in the sample at time t is calculated via Eq. (3):

$$P_{t-CaCO_3} = \frac{m_{t-CaCO_3}}{m_p} \tag{3}$$

Here, P_{t-CaCO_3} is the purity of the $CaCO_3$ in the sample of products, and m_p is the mass of the sample of products.

$$\rho_t = \frac{P_{t-CaCO_3}}{P_{C-CaCO_3}} \tag{4}$$

Where ρ_t represents the CO_2 mineralization efficiency of FGDG and P_{C-CaCO_3} represents the purity of $CaCO_3$ when FGDG was 100% mineralized. The purity of the $CaSO_4$ in FGDG used in the study was 97%, as determined by wet analysis. Therefore, the purity of the reaction product should be 95.9% for 100% mineralization.

Results and discussion

Effect of reaction parameters on CO_2 mineralization efficiency

Effect of the initial ionic strength of waste Lye on the CO_2 mineralization efficiency

The effects of the initial ionic strength of waste lye on CO_2 mineralization were evaluated by varying initial ionic strengths, which were 10^{-12} mol·L^{-1}, 5×10^{-9} mol·L^{-1}, and 10^{-2} mol·L^{-1} (denoted as $I_{10}{}^{-12}$, $I_{5\times10}{}^{-9}$ and $I_{10}{}^{-2}$, respectively).

Figure 4a shows the variation in slurry pH with time. As CO_2 was introduced into the slurry, the reaction began, and OH^- ions in the slurry were consumed, resulting in a decrease in the pH of the slurry. The pH of the slurry gradually stabilized after approximately 6 min of continuous reaction. Under all conditions, the CO_2 mineralization efficiency and slurry pH tended to stabilize at around 6 min, which was considered the termination point of the mineralization reaction, as shown in Fig. 4a. Higher ionic strength increases ion collision frequency and accelerates Ca^{2+} leaching from FGDG, thereby promoting mineralization kinetics at the early stage. Despite varying initial ionic strengths, the reaction is ultimately limited by CO_2 dissolution and diffusion rates in the bubble column reactor. When the system reaches the equilibrium, the reaction process tends to be stabilized regardless of the ionic strength. At this stage, the reaction terminates regardless of initial ionic strength, as the mineralized system becomes limited by the availability of reactants rather than kinetic factors[29].

When the ionic strength decreases, the final pH of the slurry drop due to the protonation of OH^- during CO_2 dissolution:

$$CO_2 + OH^- \rightarrow HCO_3{}^- \quad (pH \sim 10-12)$$

$$HCO_3{}^- + OH^- \rightarrow CO_3{}^{2-} + H_2O \quad (pH \sim 7-9)$$

At higher ionic strengths (10^{-2} mol·L^{-1}, the buffering capacity of the waste lye increases due to the Le Chatelier principle: excess Na^+ shifts the carbonate equilibrium toward $CO_3{}^{2-}$ formation, maintaining a near-neutral pH (~7) even after OH^- depletion[30]. The final pH of the slurry slightly increased as the initial ionic strength of the waste lye increased. The final pH increases as the initial ionic strengths of the waste lye increases. This phenomenon is attributed to activity coefficient effects. According to the Davies equation, the activity coefficient of OH^- decreases at high ionic strengths due to ion pairing effects, which reduces the effective OH^- concentration, while the analytical (total) OH^- concentration remains unchanged. This phenomenon aligns with the observed pH trend[31]. The CO_2 mineralization efficiency of FGDG was also affected by the initial ionic strength of the waste lye. After approximately 6 min of reaction, the mineralization reaction was essentially complete, and then the reaction approached the saturation state, as shown in Fig. 4b. The CO_2 mineralization efficiency of FGDG increased slightly with the continuous influx of CO_2 after 6 min of reaction. Increasing the ionic strength of waste lye from 10^{-12} mol·L^{-1} to 10^{-2} mol·L^{-1} enhanced the CO_2 mineralization efficiency from 9.8% to 67.76%. According to collision theory, when the initial ionic strength of the spent lye reaches 10^{-2} mol·L^{-1}, the number of Na^+ and OH^- ions per unit volume is large, leading to a higher frequency of effective collisions between different ions per unit time and an increase reaction rate[32]. Moreover, as the concentration of OH^- in the slurry increases, the amount of Ca^{2+} leached also increases, intensifying the mineralization reaction and resulting in higher CO_2 mineralization efficiency Luo verified this conclusion from the perspective of pH[33].

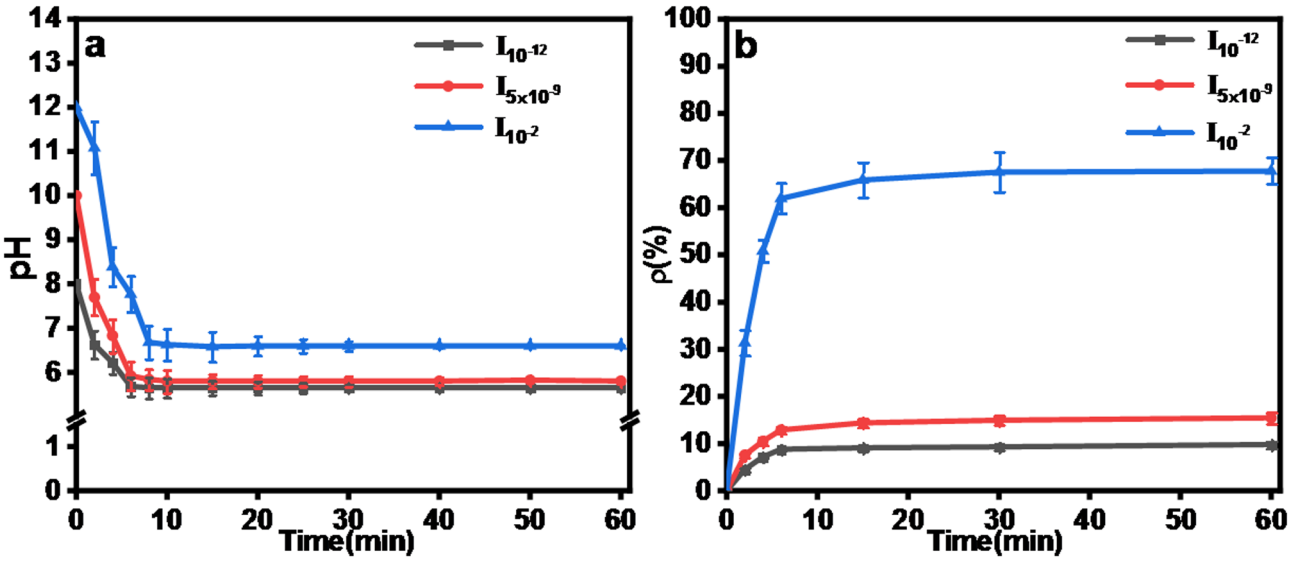

Fig. 4. (**a**) pH value curves with respect to time and (**b**) Effect of the initial ionic strength of waste lye on the CO_2 mineralization efficiency (Conditions: 40 °C temperature, 20 L·h^{-1} CO_2 flow rate, 30 cm liquid level.).

The above results indicated that a high ionic strength of waste lye would be beneficial for the mineralization reaction to generate higher purity $CaCO_3$ in the products, and the mineralization reaction would be more thorough. A high ionic strength of waste lye is ideal for increasing CO_2 mineralization efficiency[34,35].

Effect of the CO_2 flow rate on the CO_2 mineralization efficiency

The effects of the CO_2 flow rate on CO_2 mineralization were evaluated by varying the CO_2 flow rates which were 20, 40 and 60 $L{\cdot}h^{-1}$ (denoted as r20, r40 and r60, respectively).

In all the samples, the pH of the slurry decreased until it stabilized at 7 after around 10 min, as shown in Fig. 5a. The CO_2 mineralization efficiency also tended to stabilize when the reaction lasted for about 10 min. However, the final CO_2 mineralization efficiency decreased from 67.76% to 38.35% when the CO_2 flow rate increased from 20 $L{\cdot}h^{-1}$ to 60 $L{\cdot}h^{-1}$, as shown in Fig. 5b. Increasing the CO_2 flow rate was not conducive to achieving high CO_2 mineralization efficiency of FGDG. This may be attributed to the increase in bubble diameter and the decrease in the contact area between CO_2 and the slurry at higher CO_2 flow rate[36,37]. According to Henry's Law, the dissolution of CO_2 into the liquid phase is directly proportional to the interfacial area. A reduced interfacial area limits the dissolution of CO_2 into the waste lye, thereby decreasing the availability of dissolved CO_2 for the mineralization reaction[38]. Additionally, the contact time between CO_2 bubbles and the liquid phase decreased at higher flow rates. This is because the bubbles rise more rapidly through the reactor, reducing the time available for CO_2 to dissolve and react with Ca^{2+} ions leached from FGDG, which is unfavorable for CO_2 mineralization.

Effect of the reaction temperature on the CO_2 mineralization efficiency

The effects of the reaction temperature of waste lye on CO_2 mineralization were evaluated by varying the reaction temperature of the waste lye. The CO_2 mineralization efficiency tended to stabilize, and the pH of the slurry reached 7 after ~ 10 min when the reaction temperature were 40 °C and 60 °C, as shown in Fig. 6a. The time which the CO_2 mineralization efficiency and pH of the slurry reached stability increased to about 15 min at 80 °C. When the reaction temperature was increased from 40 °C to 60 °C, the CO_2 mineralization efficiency increased from 67.76% to 78.31%. When the reaction temperature was increased from 60 °C to 80 °C, the CO_2 mineralization efficiency decreased from 78.31% to 55.62%, as shown in Fig. 6b.

From the perspective of ion collision, when the reaction temperature increased from 40 °C to 60 °C, the collision frequency of ions increased, and the effective number of collisions per unit time increased resulting in an increase in the reaction rate[32,39]. Moreover, the increase in temperature was conducive to the precipitation of CO_2 mineralization components in FGDG and improved the CO_2 mineralization efficiency[36]. At the same time, the reaction rate constant (K) increased exponentially with temperature, as described by Eq. (5):

$$K = A \times e^{\frac{-E_a}{RT}} \tag{5}$$

where E_a is the activation energy, A is the pre-exponential factor, R is the gas constant, and T is the temperature. For FGDG mineralization, the activation energy barrier for Ca^{2+} release and carbonate formation was more readily overcome at elevated temperatures[40].

However, excessively high temperatures would reduce the CO_2 dissolution rate, and the CO_3^{2-} concentration in the solution decreased, resulting in a decline in the reaction rate and CO_2 mineralization efficiency. According to Henry's Law, the solubility of CO_2 in water decreased with rising temperature. At 80 °C, CO_2 gas-liquid mass transfer was hindered, reducing the availability of dissolved CO_2 for FGDG. The carbonation reaction is exothermic. Le Chatelier's principle predicts that higher temperatures shift the equilibrium toward reactant dissociation, suppressing $CaCO_3$ precipitation, which is consistent with previous results in the literature[41].

Effects of the liquid level on the CO_2 mineralization efficiency

The effects of the liquid level of the waste lye in the reactor on CO_2 mineralization were evaluated by varying the liquid level which was 30, 40 and 50 cm. The difference in liquid level can lead to different capacities of waste lye in the reactor during the experiment. Therefore, it was necessary to change the quantity of FGDG added, to ensure that the solid–liquid ratio remained constant and that the experiment proceeded smoothly. The change

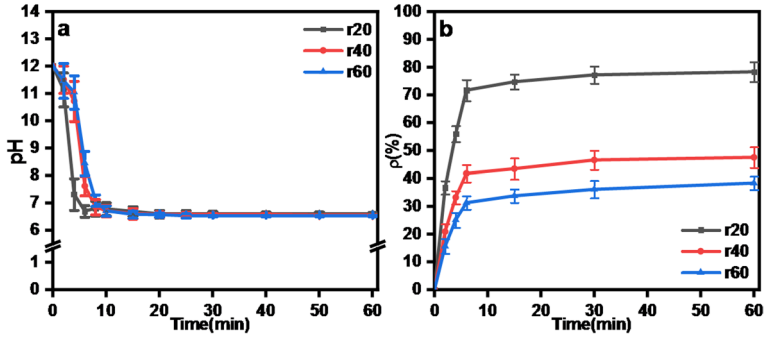

Fig. 5. (**a**) pH value curves depending on time and (**b**) Effect of CO_2 flow rate on CO_2 mineralization efficiency (Conditions: 40 °C temperature, 10^{-2} $mol{\cdot}L^{-1}$ initial ionic strength of waste lye, 30 cm liquid level.).

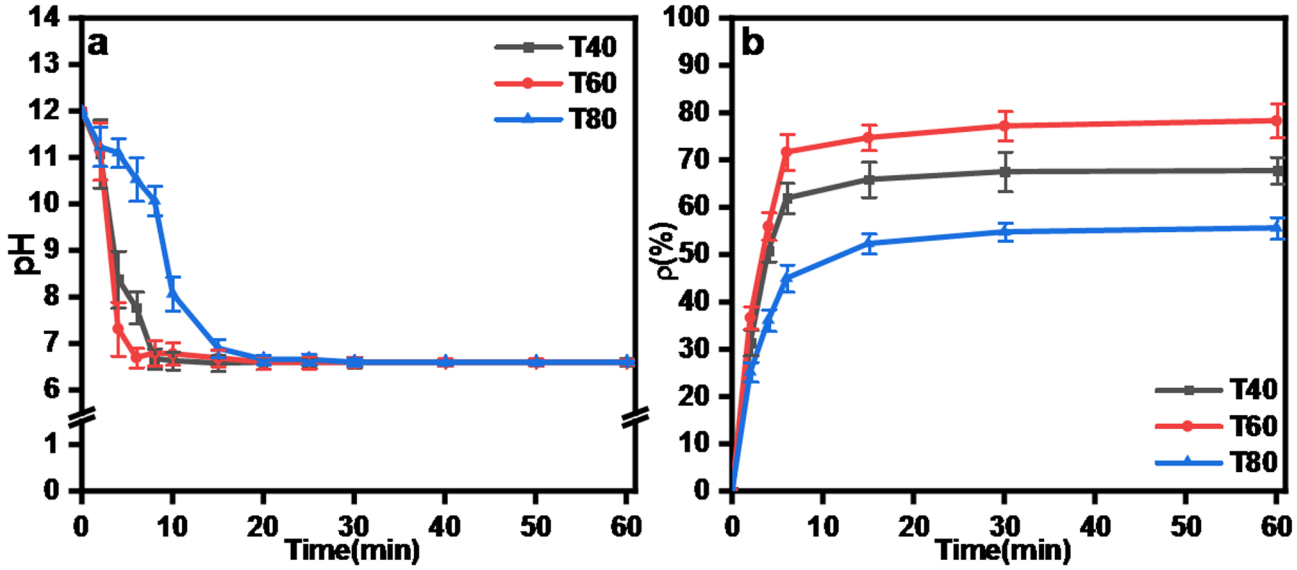

Fig. 6. (**a**) pH value curves with respect to time and (**b**) Effect of reaction temperature on the mineralization efficiency (Conditions: 20 L·h^{-1} CO_2 flow rate, 10^{-2} mol·L^{-1} initial ionic strength of waste lye, 30 cm liquid level.).

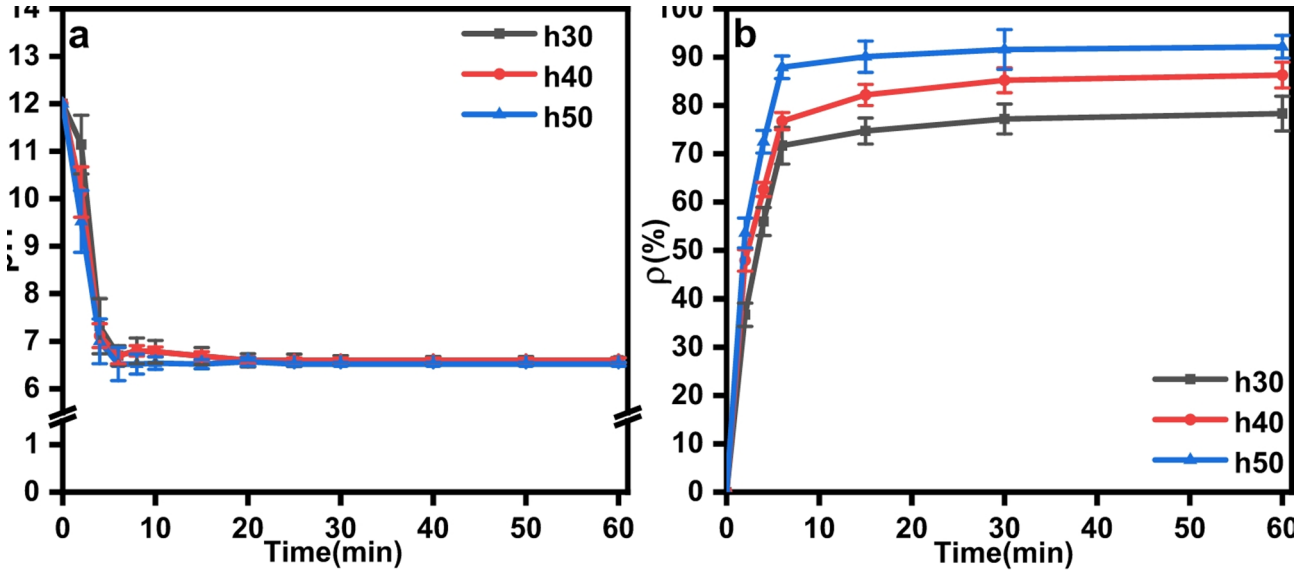

Fig. 7. (**a**) pH value curves as a function of time and (**b**)Effect of liquid level on mineralization efficiency (Conditions: 60 °C temperature, 20 L·h^{-1} CO_2 flow rate, 10^{-2} mol·L^{-1} initial ionic strength of waste lye.).

in the liquid level was not significant. After approximately 6 min of reaction, the pH of the slurry decreased to 7, and the decline curve was consistent, as shown in Fig. 7a. At the same time, the CO_2 mineralization efficiency tended to stabilize after about 6 min of reaction. When the liquid level increased from 30 cm to 50 cm, the CO_2 mineralization efficiency increased from 78.31% to 92.15%, as shown in Fig. 7b. According to penetration theory, the gas-liquid contact time (t_c) is proportional to the liquid level (h):

$$t_c \propto \frac{h}{u_g} \tag{6}$$

where u_g is the bubble rise velocity. A taller liquid column allows CO_2 bubbles to remain in contact with the slurry for longer, increasing the dissolution of CO_2 and subsequent reaction with Ca^{2+} ions. This extended contact time ensures more complete conversion of CO_2 to carbonate species (HCO_3^-/CO_3^{2-}), thereby

improving mineralization efficiency[42]. The above results indicate that a high liquid level is favorable for high CO_2 mineralization efficiency[43].

Effect of reaction parameters on product particle size

Effect of the initial ionic strength of waste Lye on product particle size

The effects of the initial ionic strength of the waste lye on the particle size distribution of the products were investigated by changing the initial ionic strength of the waste lye (10^{-12} mol·L^{-1}, 5×10^{-9} mol·L^{-1}, 10^{-2} mol·L^{-1}). Figure 8 shows the particle size distributions of the products generated under different initial ionic strengths of the waste lye. The products exhibited a bimodal particle size distribution, with peak values at approximately 2 μm and 25 μm. When the initial ionic strengths of the waste lye were 10^{-12} mol·L^{-1}, 5×10^{-9} mol·L^{-1}, and 10^{-2} mol·L^{-1}, the d_{50} values of the products were 13.4 μm, 11.7 μm and 10.4 μm, respectively. The d_{50} of the products decreased by 29.97% as initial ionic strength of the waste lye increased from 10^{-12} mol·L^{-1} to 10^{-2} mol·L^{-1}. Higher ionic strength increased the concentration of free ions in the waste lye, accelerating the nucleation process. This resulted in a larger number of smaller $CaCO_3$ nuclei forming simultaneously, which limited subsequent crystal growth due to competitive ion consumption[44]. Therefore, an increase in the initial ionic strength of waste lye is favorable for obtaining small particle products.

Effects of the CO_2 flow rate on product particle size

The CO_2 flow rate also significantly influenced the particle size distribution of the products. Figure 9 illustrates the effect of the CO_2 flow rate on the particle size distribution. At a flow rate of 20 L·h^{-1}, the product exhibited bimodal peaks at 1.9 μm and 28.4 μm, with a d_{50} value of 10.4 μm. When the CO_2 flow rates were increased to 40 L·h^{-1} and 60 L·h^{-1}, the bimodal peak values shifted to approximately 3.4 μm and 32.2 μm, with d_{50} values of 17.1 μm and 19.4 μm, respectively. As the CO_2 flow rate increased from 20 L·h^{-1} to 60 L·h^{-1}, the bimodal particle sizes distribution shifted to the right. And the d_{50} of the products increased by 86.55%. These results indicate that higher CO_2 flow rates increased the proportion of large particles in the products, which hindered the formation of small particles.

A higher CO_2 flow rate accelerated crystal growth, whereas a lower flow rate favored the formation of smaller particles. Increased CO_2 flow rates intensified the churning and stirring of the slurry[45], leading to greater drag forces on the particles. As a result, the larger and heavier particles were more likely to reach higher liquid levels.

Additionally, the higher CO_2 flow rates introduced turbulence and shear stress within the reactor. According to colloidal theory, excessive turbulence can disrupt nascent $CaCO_3$ crystals, resulting in a higher proportion

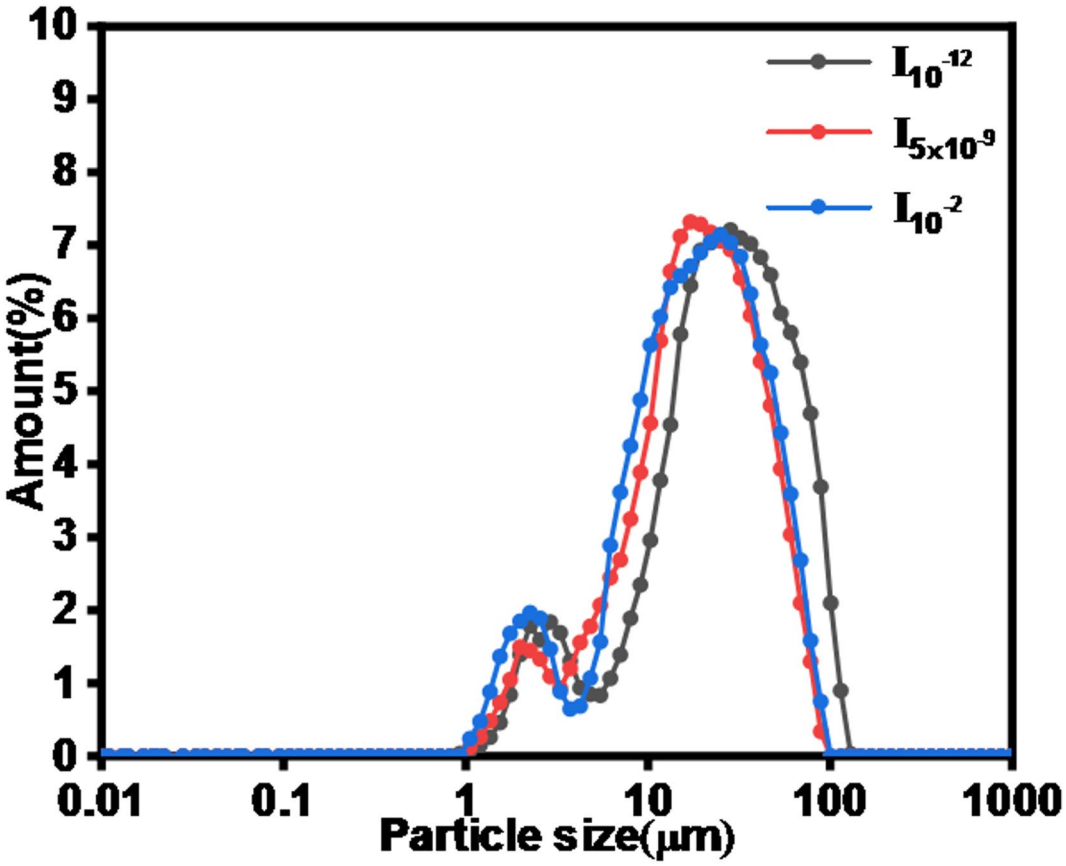

Fig. 8. Effect of the initial ionic strength of waste lye on the particle size distribution of the products (Conditions: 40 °C temperature, 20 L·h^{-1} CO_2 flow rate, 30 cm liquid level).

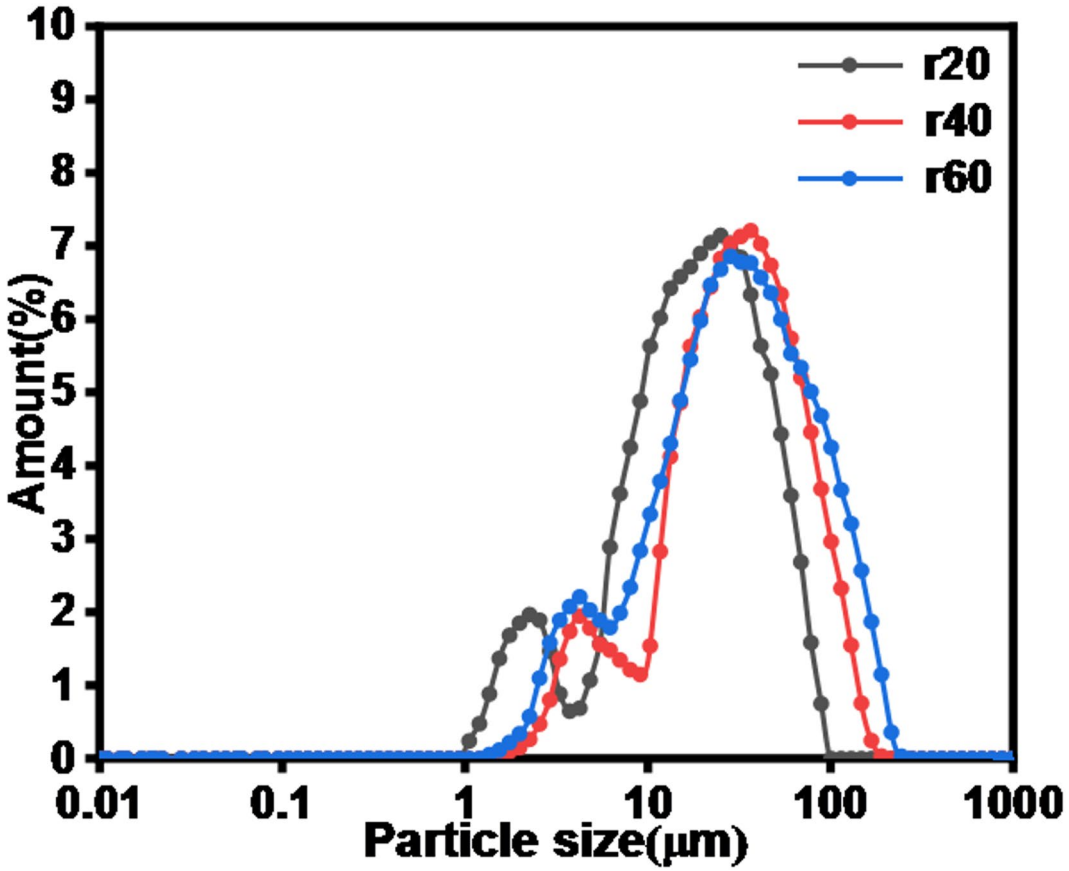

Fig. 9. Effect of the CO_2 flow rate on the particle size distribution (Conditions: 40 °C temperature, 10^{-2} mol·L^{-1} initial ionic strength of waste lye, 30 cm liquid level.).

of larger, less reactive particles. This observation aligns our findings that higher flow rates increased the particle size of the mineralization products[46].

Effect of reaction temperature on product particle size

Figure 10 shows the effect of the reaction temperature of waste lye on the particle size distribution of the products. Under all tested conditions, the products exhibited a bimodal distribution, with bimodal peak values ranging from 2.3 μm to 2.9 μm and 22.5 μm to 28.4 μm. The d_{50} values of the products varied between 10.4 μm and 11.3 μm. These results indicate that the reaction temperature had no significant effect on the particle size distribution of the products[47].

Effect of liquid level on products particle size

In this stage, the influence of the liquid level on the particle size distribution of the products was studied by varying the liquid level inside the reactor. Figure 11 shows a bimodal distribution of the products under different liquid level conditions. When the liquid level was 30 cm, the bimodal peak values of the products were 1.9 μm and 28.4 μm and the d_{50} value was 10.4 μm. at a liquid level of 40 cm, the bimodal peak values shifted to 2.5 μm and 11.7 μm and the d_{50} value decreased to 6.2 μm. Further increasing the liquid level to 50 cm resulted in bimodal peak values of 1.5 μm and 7.1 μm, with a d_{50} value of 4.2 μm. When the liquid level was raised from 30 cm to 50 cm, a 62.83% reduction in the d_{50} of the products was observed. Additionally, the peaks corresponding to smaller particle sizes became more pronounced, and the overall particle size distribution shifted to the left as the liquid level increased. The liquid level affects the turbulent shear stress (τ) within the reactor, which plays critical role in crystal nucleation and growth[48].

$$\tau \propto \rho u\prime^2 \tag{7}$$

Where ρ is fluid density and u' is turbulent velocity fluctuation. At higher liquid levels, increased turbulence generates stronger shear forces. These enhanced shear forces disrupt the growth of $CaCO_3$ crystals, promoting nucleation over Ostwald ripening. This results in smaller particle sizes, as observed in our experiments. Furthermore, higher liquid levels reduce the settling velocity of FGDG particles (as described by Stokes' law), maintaining a homogeneous slurry. This prevents particle agglomeration and maximizes the reactive surface

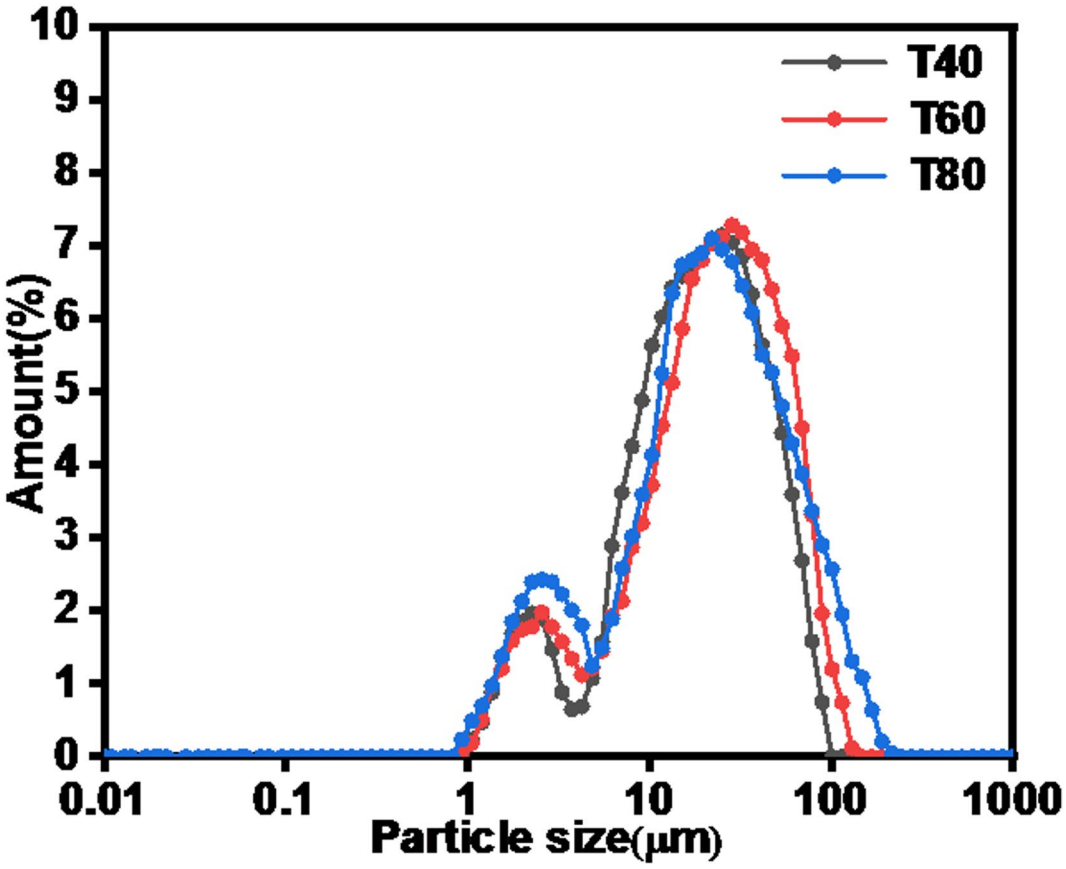

Fig. 10. Effect of the reaction temperature on the particle size distribution (Conditions: 20 L·h^{-1} CO_2 flow rate, 10^{-2} mol·L^{-1} initial ionic strength of waste lye, 30 cm liquid level).

area of $CaSO_4 \cdot 2H_2O$ for Ca^{2+} leaching[49]. The above experimental results demonstrate that a higher liquid level reduces the proportion of large particles in the products, leading to smaller particle sizes.

Characterization

Characterization and analysis of the product

After 60 min of mineralization, $CaSO_4$, the main component of dried FGDG, was converted to $CaCO_3$, the main component of the mineralization product. However, a small amount of $CaSO_4$ remained in the mineralization product, as shown in Fig. 12. In gas-liquid reactor systems, gypsum particles undergo Stokes sedimentation, leading to a significant increase in particle concentration within the bottom region and forming a diffusion-limited reaction zone. Turbulent characteristics within the reactor (e.g., Taylor-scale vortices) influence particle collision frequency and mass transfer efficiency, with this process exhibiting multi-scale coupling effects. Therefore, the variation of the proportion of incomplete $CaSO_4$ conversion and its potential impact on product properties are complex and multifaceted[50]. Figure 13a presents a scanning electron microscope (SEM) image of the FGDG. The carbonization products consisted of amorphous nanosized particles with an aggregate structure[18,51], in contrast to the original diamond-shaped morphology of FGDG, as shown in Fig. 13b, c. Energy-dispersive X-ray spectroscopy (EDS) analysis of the carbonized products, shown in Fig. 13d, revealed that they primarily contained Ca, C, and O, confirming the formation of $CaCO_3$ aggregates.

Conclusion

The study was focused on that FGDG mixed with waste NaOH lye can function as an absorbent to capture CO_2 and then $CaCO_3$ subsequently produced through the gas-liquid- solid phase reaction. The CO_2 mineralization efficiency increased from 9.8% to 67.76% and the d_{50} of the products decreased from 13.4 μm to 10.4 μm with the elevated ionic strength. Reducing the CO_2 flow rate can prolong the gas-liquid-solid contact time, improved the CO_2 mineralization efficiency from 38.35% to 67.76%, and reduced the d_{50} of the products from 19.4 μm to 10.4 μm. The reaction temperature significantly influenced the CO_2 mineralization process. The CO_2 mineralization efficiency initially increased and then decreased with rising reaction temperature, reaching an optimal efficiency of 78.31% at 60 °C. However, the reaction temperature had no significant effect on the particle size of the products. The elongated sampling tube can increase the liquid level, increased the CO_2 mineralization efficiency from 78.31% to 92.15%, and reduced the d_{50} of the products from 10.4 μm to 4.2 μm. The maximum CO_2 mineralization efficiency was 92.15% and the d_{50} of the products was 4.2 μm under optimized conditions

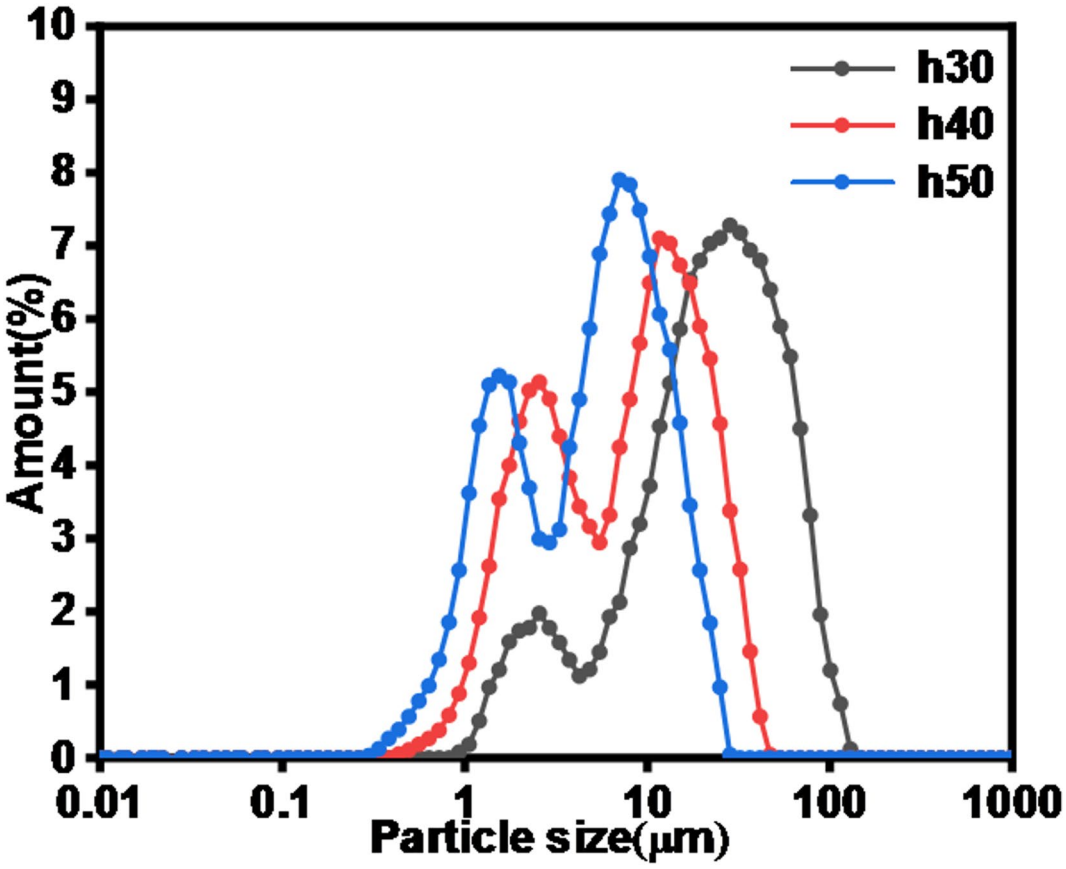

Fig. 11. Effect of the liquid level on the particle size distribution (Conditions: 60 °C temperature, 20 $L{\cdot}h^{-1}$ CO_2 flow rate, 10^{-2} $mol{\cdot}L^{-1}$ initial ionic strength of waste lye.).

(ionic strength: 10^{-2} $mol{\cdot}L^{-1}$, CO_2 flow rate: 20 $L{\cdot}h^{-1}$, temperature: 60 °C, liquid level: 50 cm). The solid in the slurry was also transformed from columnar $CaSO_4$ crystals into clusters of $CaCO_3$ aggregates. In conclusion, this study successfully demonstrated an efficient method for CO_2 mineralization using FGDG and waste NaOH lye, offering a sustainable solution for carbon capture and utilization.

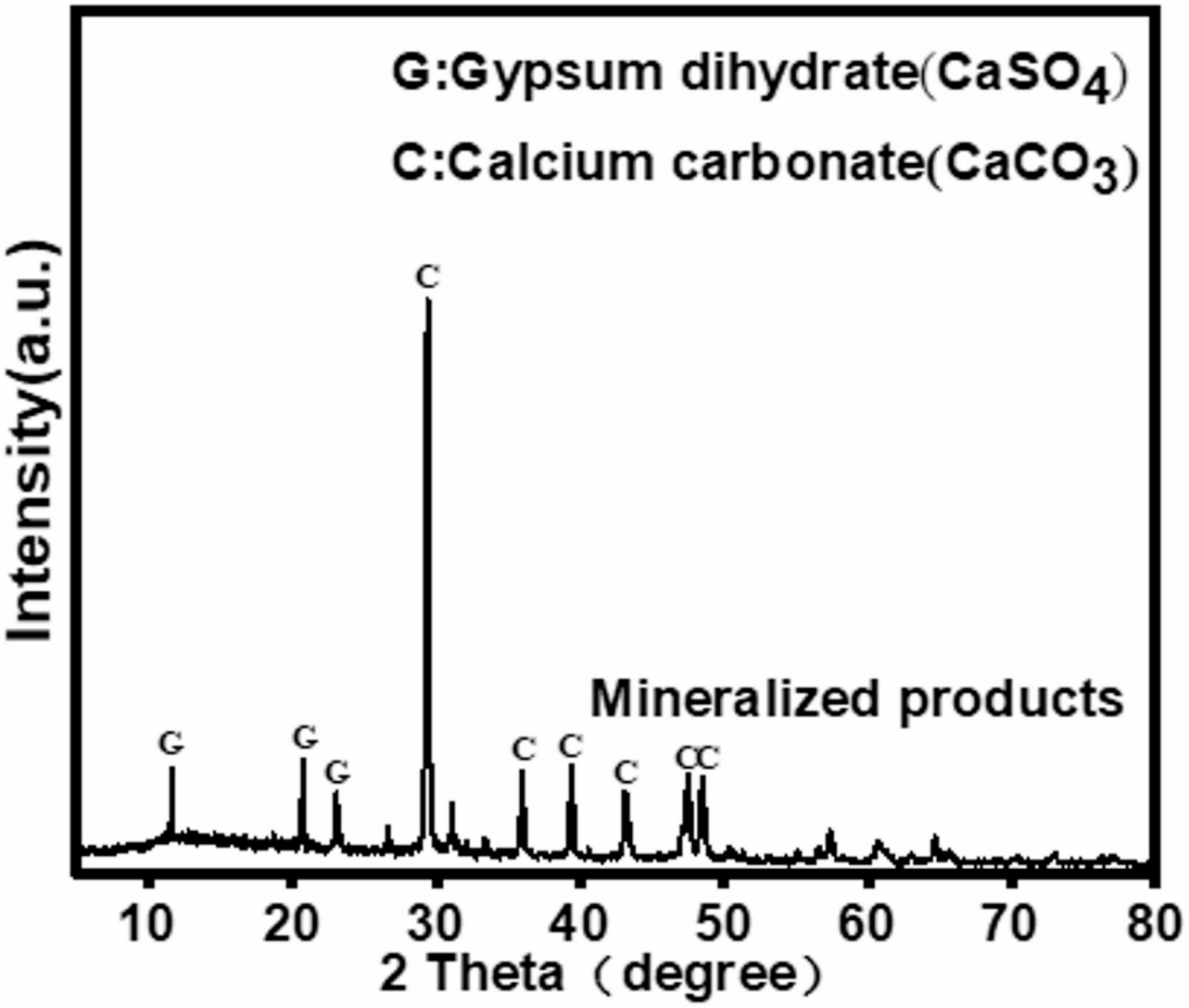

Fig. 12. XRD patterns of the mineralized product.

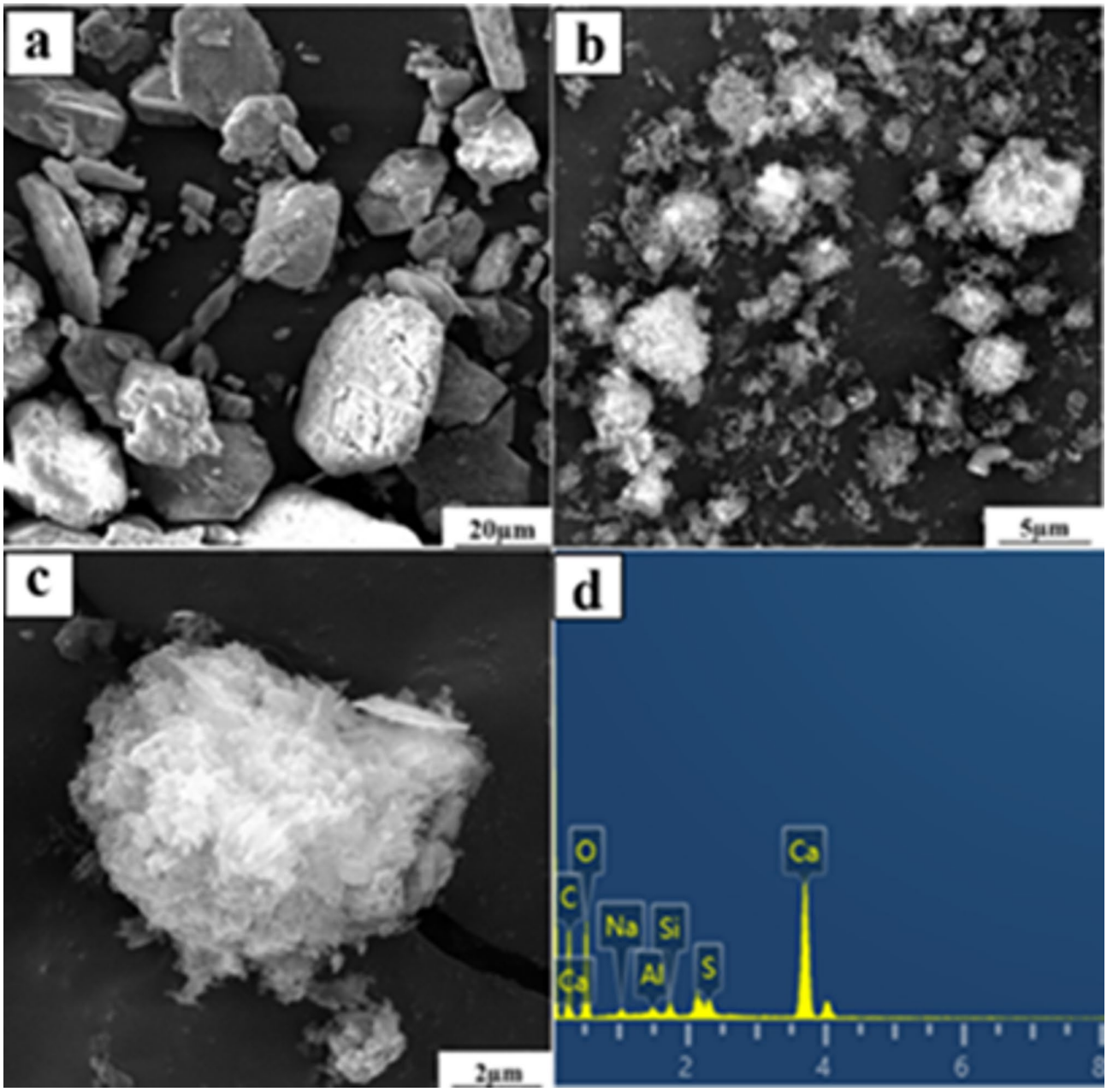

Fig. 13. (**a**) SEM images of raw FGDG; (**b**,**c**) SEM images of mineralization products; (**d**) EDS mapping of mineralization products.

Data availability

All data generated or analysed during this study are included in this published article.

Received: 17 November 2024; Accepted: 7 May 2025
Published online: 21 May 2025

References

1. Dahlke, F. T. et al. Northern Cod species face spawning habitat losses if global warming exceeds 1.5°C. *Sci. Adv.* **4**, 8821 (2018).
2. Zhu, C. et al. Carbon dioxide (CO_2) levels this century will alter the protein, micronutrients, and vitamin content of rice grains with potential health consequences for the poorest rice-dependent countries. *Sci. Adv.* **4**, 1012 (2018).
3. Schwartz, S. E. Resource Letter GECC-2: The greenhouse effect and climate change: The intensified greenhouse effect. *Am. J. Phys.* **86**, 645–656 (2018).
4. Longgui, X. et al. Research progress of carbon sequestration technology of industrial solid waste gypsum. *Phosphate Compound Fertil.* **37**, 32–35 (2022).
5. Jiang, K. & Ashworth, P. The development of carbon capture utilization and storage (CCUS) research in China: A bibliometric perspective. *Renew. Sustain. Energy Rev.* **138**, 110521 (2021).

6. Seifritz, W. CO_2 disposal by means of silicates. *Nature* **345**, 486–486 (1990).
7. Jingwei, R. et al. Research status and application potential of CO_2 mineralization. *Earth Sci.* **45**, 2413–2425 (2020).
8. Pandey, S., Srivastava, V. & Kumar, V. Comparative thermodynamic analysis of CO_2 based dimethyl carbonate synthesis routes. *Can. J. Chem. Eng.* **99**, 23893 (2020).
9. Pan, S. Y. et al. CO_2 mineralization and utilization by alkaline solid wastes for potential carbon reduction. *Nat. Sustain.* **3**, 1–7 (2020).
10. Ćwik, A., Casanova, I., Rausis, K., Koukouzas, N. & Zarębska, K. Carbonation of high-calcium fly ashes and its potential for carbon dioxide removal in coal fired power plants. *J. Clean. Prod.* **202**, 1026–1034 (2018).
11. Ho, H. J., Iizuka, A. & Shibata, E. Utilization of low-calcium fly ash via direct aqueous carbonation with a low-energy input: Determination of carbonation reaction and evaluation of the potential for CO_2 sequestration and utilization. *J. Environ. Manag.* **288**, 112411 (2021).
12. Wang, B. et al. CO_2 sequestration: High conversion of gypsum into $CaCO_3$ by ultrasonic carbonation. *Environ. Chem. Lett.* **18**, 1369–1377 (2020).
13. Azdarpour, A., Afkhami Karaei, M., Hamidi, H., Mohammadian, E. & Honarvar, B. CO_2 sequestration through direct aqueous mineral carbonation of red gypsum. *Petroleum* **4**, 398–407 (2018).
14. Altiner, M., Top, S., Kaymakoğlu, B., Seçkin, İ. Y. & Vapur, H. Production of precipitated calcium carbonate particles from gypsum waste using venturi tubes as a carbonation zone. *J. CO_2 Util.* **29**, 117–125 (2019).
15. Li, H., Tang, Z., Li, N., Cui, L. & Mao, X. Mechanism and process study on steel slag enhancement for CO_2 capture by seawater. *Appl. Energy*. **276**, 115515 (2020).
16. Yuan, Y. et al. Method for rapid mineralization of CO_2 with carbide slag in the constant-pressure and continuous-feed way and its reaction heat. *Powder Technol.* **398**, 117148 (2022).
17. Liu, S., Liu, W., Jiao, F., Qin, W. & Yang, C. Production and resource utilization of flue gas desulfurized gypsum in China—A review. *Environ. Pollut.* **288**, 117799 (2021).
18. Lee, M., Jang, Y. N., Ryu, K., Kim, W. & Bang, J. H. Mineral carbonation of flue gas desulfurization gypsum for CO_2 sequestration. *Energy* **47**, 370–377 (2012).
19. Wang, B., Pan, Z., Du, Z., Cheng, H. & Cheng, F. Effect of impure components in flue gas desulfurization (FGD) gypsum on the generation of polymorph $CaCO_3$ during carbonation reaction. *J. Hazard. Mater.* **369**, 236–243 (2019).
20. Ding, W., Qiao, J., Zeng, L., Sun, H. & Peng, T. Desulfurization gypsum carbonation for CO_2 sequestration by using recyclable ammonium salt. *Int. J. Greenh. Gas Control.* **123**, 103843 (2023).
21. Wang, Y. et al. Amine-promoted gypsum carbonation for efficient CO_2 capture and selective synthesis of $CaCO_3$ polymorph integrating with amine regeneration by bipolar membrane electrodialysis. *Chem. Eng. J.* **478**, 147335 (2023).
22. Chang, E. E. et al. Carbonation of basic oxygen furnace slag with metalworking wastewater in a slurry reactor. *Int. J. Greenh. Gas Control.* **12**, 382–389 (2013).
23. Valdez-Castro, L. et al. Capture of CO_2 through phosphogypsum and Lye residues from the Olive industry. *J. CO_2 Util.* **72**, 102504 (2023).
24. Ma'mun, S., Chafidz, A., Indrayanto, E. & Setiawan, P. K. The effect of ionic strength on protonation constant of monoethanolamine in water at 303 K. *J. Phys. Conf. Ser.* **1295**, 1742–1748 (2019).
25. Nyong, B. E., Abeng, F. E., Ushie, O. A., Bassey, B. J. & Edim, M. M. Kinetics mechanism and thermodynamic study of the oxidation of iodide ion by dichromate ion in acidic medium. *J. Appl. Sci. Environ. Manag.* **24**, 821–826 (2020).
26. Tan, W., Zhang, Z., Li, H., Li, Y. & Shen, Z. Carbonation of gypsum from wet flue gas desulfurization process: Experiments and modeling. *Environ. Sci. Pollut. Res. Int.* **24**, 8602–8608 (2017).
27. Pane, I. & Hansen, W. Investigation of blended cement hydration by isothermal calorimetry and thermal analysis. *Cem. Concrete Res.* **35**, 1155–1164 (2005).
28. Lin, H., Liu, W., Zhang, D., Chen, B. & Zhang, X. Study on the degradation mechanism of mechanical properties of red sandstone under static and dynamic loading after different high temperatures. *Sci. Rep.* **15**, 11611 (2025).
29. Li, Z. et al. Dissolution kinetics of iron sulfide minerals in alkaline solutions. *Cem. Concrete Res.* **193**, 107850 (2025).
30. Yin, H. et al. Alloying effect-induced electron polarization drives nitrate electroreduction to ammonia. *Chem. Catal.* **1**, 1088–1103 (2021).
31. McHedlov-Petrossyan, N. O. The Davies equation of state of ionic surfactant adsorbed monolayer and related problems. *Colloids Surf. Physicochem. Eng. Aspects*. **537**, 325–333 (2018).
32. Chahiyan, H., Gharib, F. & Farajtabar, A. Thermodynamic studies on solubility and protonation constant of acetaminophen at different ionic strengths and various temperatures. *J. Mol. Liq*. **199**, 137–142 (2014).
33. Luo, X. et al. A green approach to prepare polymorph $CaCO_3$ for clean utilization of salt gypsum residue and CO_2 mineralization. *Fuel* **333**, 126305 (2023).
34. Ebrahimi, A. et al. Sustainable transformation of fly ash industrial waste into a construction cement blend via CO_2 carbonation. *J. Clean. Prod.* **156**, 660–669 (2017).
35. Muljani, S., Setyawan, H. & Nugraha, R. E. Bubble formation phenomenon on the absorber column for CO_2 absorption and to produce precipitated silica sodium carbonate. *RSC Adv.* **13**, 33471–33483 (2023).
36. Xiangli, N., Fenghua, L. & Enzhu, H. CO_2 sequestration by red mud under coupling effect of ultrasonic wave and mechanical agitation. *Environ. Eng.* **12**, 2973–2979 (2018).
37. Jo, H. Y., Ahn, J. H. & Jo, H. Evaluation of the CO_2 sequestration capacity for coal fly Ash using a flow-through column reactor under ambient conditions. *J. Hazard. Mater.* **241–242**, 127–136 (2012).
38. Ghaslani, D., Eshaghi Gorji, Z., Ebrahimpoor Gorji, A. & Riahi, S. Descriptive and predictive models for Henry's law constant of CO_2 in ionic liquids: A QSPR study. *Chem. Eng. Res. Des.* **120**, 15–25 (2017).
39. Massoumıları, Ş. & Velioğlu, S. Theoretical perspectives on CO_2 separation by ionic liquids: Addressing crucial questions. *Sep. Purif. Technol.* **354**, 129397 (2025).
40. Lamadrid, H. M. et al. Effect of water activity on rates of serpentinization of olivine. *Nat. Commun.* **8**, 16107 (2017).
41. Zhao, H. et al. Experimental study of enhanced phosphogypsum carbonation with ammonia under increased CO_2 pressure. *J. CO_2 Util.* **11**, 10–19 (2015).
42. Janssens, P., Poissonnier, J., Bos, R. & Thybaut, J. W. Penetration-model-based criteria for the identification of the instantaneous regime for irreversible gas-liquid reactions. *Chem. Eng. J.* **502**, 157708 (2024).
43. Haghnegahdar, M. R., Hatamipour, M. S. & Rahimi, A. Mathematical modeling of CO_2 capture in a semi-dry spouted bed reactor. *Sep. Purif. Technol.* **80**, 509–518 (2011).
44. Hamdi, R. & Tlili, M. M. Influence of foreign salts and antiscalants on calcium carbonate crystallization. *Crystals* **13**, 516 (2023).
45. Lu, S. Q., Lan, P. Q. & Wu, S. F. Preparation of nano-$CaCO_3$ from phosphogypsum by gas–liquid–solid reaction for CO_2 sorption. *Ind. Eng. Chem. Res.* **55**, 10172–10177 (2016).
46. Tavakoli, A., Rahimi, K., Saghandali, F., Scott, J. & Lovell, E. Nanofluid preparation, stability and performance for CO_2 absorption and desorption enhancement: A review. *J. Environ. Manag.* **313**, 114955 (2022).
47. Librandi, P. et al. Carbonation of steel slag: Testing of the wet route in a pilot-scale reactor. *Energy Procedia*. **114**, 5381–5392 (2017).
48. Lu, J., Guo, Y., Xin, Y., Yang, X. & Li, J. Turbulence-assisted shear regulatable synthesis of ag nanoparticles using a counter axial-swirling impinging jet flow reactor. *Chem. Eng. Sci.* **308**, 121418 (2025).

49. Ozenda, O., Saramito, P. & Chambon, G. Shear-induced migration in concentrated suspensions: Particle mass conservation, contact pressure and jamming. *J. Non-Newtonian Fluid Mech.* **304**, 104805 (2022).
50. Krishnamoorthy, P. Sedimentation model and analysis for differential settling of two-particle-size suspensions in the Stokes region. *Int. J. Sediment. Res.* **25**, 119–133 (2010).
51. Song, K., Kim, W., Bang, J. H., Park, S. & Jeon, C. W. Polymorphs of pure calcium carbonate prepared by the mineral carbonation of flue gas desulfurization gypsum. *Mater. Des.* **83**, 308–313 (2015).

Acknowledgements

This work was supported by the National Science Foundation of China (No. 51678291), the Major Fundamental Science Research of Universities in Jiangsu Province (No. 23KJA610003) and an innovative team of Jiangsu Province for pollution and CO_2 emission reduction in coal-fired power plants.

Author contributions

Yuliang Cao: Writing - Original Draft, Conceptualization, Formal analysis, Data Curation, Data Curation, Wenyi Tan: Supervision, Project administration, Funding acquisition, Writing - Review & Editing, ValidationTingfeng Liu: Writing - Review & EditingGuodong Chen: Resources.

Declarations

Competing interests

The authors declare no competing interests.

Additional information

Correspondence and requests for materials should be addressed to W.T.